Evaluation of Lateral Torsional Buckling Resistance Equations in AISC and AASHTO

Lakshmi Subramanian[1], Donald W. White[2]

Abstract

The lateral torsional buckling (LTB) resistance equations for rolled and welded I-sections differ considerably across the AASHTO/AISC, Eurocode, and other international design codes. These differences stem largely from residual stress and geometric imperfection sensitivity in the inelastic and elastic LTB regions of the curves. AISC/AASHTO employ a resistance calculation method by which the LTB resistance curve is clearly segmented into three distinct parts: the yield or plateau region, the inelastic buckling region and the elastic buckling region. This curve was established on the basis of experimental data, but tends to give larger strengths than common FEA test simulations in many situations. This paper evaluates the sensitivity of LTB resistances to imperfections and residual stresses on compact and on non-compact web sections. The paper then recommends nominal residual stresses and geometric imperfections to be used when conducting FEA simulations to study LTB, as well as modified LTB resistance equations based on evidence from experimental tests and test simulations.

Notation

b_{fc} = width of compression flange
D = web depth between the inside surface of the flanges
E = modulus of elasticity
E_{sh} = strain hardening modulus
ε_{sh} = strain hardening strain
ε_y = yield strain
F_u = ultimate stress of steel
F_y = yield stress of steel
F_{yr}= compression flange stress at nominal onset of yielding including the effects of residual stresses, taken as $0.7F_y$ for homogeneous doubly-symmetric I-sections in AISC/AASHTO
K = effective length factor for lateral torsional buckling
L_b = lateral unbraced length of beam/girder
L_p = limiting effective unbraced length below which the strength under uniform bending is characterized by the plateau resistance in AISC/AASHTO

---

[1] Graduate Research Assistant, Georgia Institute of Technology, <pslakshmipriya@gatech.edu>
[2] Professor, Georgia Institute of Technology, <don.white@ce.gatech.edu>

L_r = limiting effective unbraced length above which the strength under uniform bending is characterized by the theoretical elastic lateral-torsional buckling resistance in AISC/AASHTO

M_{exp}= maximum moment obtained from experimental tests as reported by authors

M_{max}= maximum moment obtained from FEA test simulations

$M_{n\,AISC}$= moment resistance calculated per AISC

M_p = plastic moment resistance

M_y = nominal yield moment capacity

R_{pc} = web plastification or cross-section effective shape factor, which accounts for the typical increase in the LTB plateau strength above M_y for non-compact and compact web sections

R_b = web bend buckling factor, which accounts for the typical decrease in the LTB plateau strength of slender web sections due to load shedding from the web to the compression flange due to web bend buckling

r_t = effective radius of gyration for lateral torsional buckling

t_{fc} = thickness of compression flange

1. Introduction

The LTB curve in AISC (2010) and AASHTO (2014) consists of three distinct regions: the plateau region, the inelastic LTB region and the elastic LTB region. The plateau resistance is the plastic moment for compact sections, while for other compact and non-compact web sections; it is the yield moment multiplied by the web plastification factor, R_{pc}. The plateau capacity for slender web sections is the yield moment reduced by the web bend buckling factor, R_b. The inelastic LTB resistance is obtained by linearly interpolating between the plateau and the elastic LTB regions. Members that have lateral unbraced lengths that fall between L_p and L_r are designed for inelastic LTB buckling, where L_p is the limiting unbraced length at which the nominal plateau strength may be achieved under uniform bending and L_r is the limiting unbraced length at which yielding effects start to influence the nominal resistance. Members with lateral unbraced lengths that are greater than L_r are designed for the theoretical elastic LTB strength.

This paper addresses a disconnect between typical FEA test simulations and the AISC/AASHTO LTB resistance equations. The AASHTO and AISC LTB strength curves are based on calibration to a wide range of experimental results as discussed by White (2008). However, the authors and other researchers (e.g., Kim (2010) and Greiner and Kaim (2001)) have observed that in many cases, the nominal LTB resistance curves recommended by AASHTO (2014) and by AISC (2010) tend to deviate substantially from the results obtained from refined test simulations. Test simulation predictions of the flexural resistance, using typical nominal residual stresses and geometric imperfections, tend to be somewhat low compared to the experimental test results, particularly for the case of uniform bending. Although the AISC/AASHTO curves represent a vast collection of experimental data, there are indications that they have some shortcomings in capturing the resistances in some areas of the design space. The curves have been found to over-predict the capacities from certain experimental tests, particularly in the inelastic LTB region (e.g., Righman (2005)). It is also true; however, that FEA simulations tend to be conservative in many cases due to the use of idealized boundary conditions, as well as assumed nominal residual stresses and geometric imperfections. The authors have conducted extensive sensitivity analyses with different magnitudes of imperfections and different residual stress patterns on members with fork boundary conditions (simply supported with twist restrained, and lateral bending and warping free at ends of the member). Sensitivity analyses also have been conducted on selected experimental tests with compact and non-compact web members subjected to uniform bending

and having more general boundary conditions. Based on these studies, the paper recommends nominal residual stresses and geometric imperfections to be used when conducting FEA simulations, such that the simulations are more representative of the mean experimental strengths captured by the AISC/AASHTO resistance equations.

The authors, while recognizing that FEA test simulations with idealized characteristics often tend to be conservative, point out some incontrovertible inconsistencies in the design resistance curves. One of the significant shortcomings of the AISC/AASHTO curves is that several types of members cannot attain their plateau moment capacities at the limiting plateau length, L_p. This is shown with the help of sensitivity studies, where FEA simulations that employ negligible geometric imperfection and zero residual stresses still fall 10 % below the capacities predicted by AISC/AASHTO equations. In addition, it is shown that the AISC/AASHTO curves indicate larger strengths than FEA simulation data throughout the inelastic LTB region in all cases involving predominant flange compressive residual stresses. Minor modifications are proposed to the current AISC/AASHTO curve to resolve the strength over-predictions at L_p and in the inelastic LTB region.

2. FEA Modeling Parameters

2.1 Mesh Discretization
The FEA test simulations discussed in this paper are full nonlinear analyses using ABAQUS (Simulia, 2013). The member flanges and web are each modeled using four-node shell elements degenerated from a 3D solid element (the S4R shell element in ABAQUS). The finite element mesh used is relatively dense with 20 elements through the web depth and 12 elements across the width of the flanges. The number of elements used along the length of the members is selected such that the shell element aspect ratios in the web are approximately equal to 1.0 within the test specimens. Transverse stiffeners are modeled using the B31 beam element in ABAQUS, which is a two-node shear deformable beam element compatible with the S4R shell element.

2.2 Material Modeling
In this paper, all members are considered to be homogenous and the yield stress of the steel, F_y, is taken as 50 ksi. Transverse stiffeners are also modeled with a yield stress of 50 ksi. The modulus of elasticity, E is taken as 29000 ksi. The material is modeled with a small tangent stiffness within the yield plateau region of $E/1000$ up to a strain-hardening strain of $\varepsilon_{sh} = 10\varepsilon_y$, where ε_y is the yield strain of the material. Beyond this strain, a constant strain-hardening modulus of $E_{sh} = E/50$ is used. The maximum stress reached in the test simulations is significantly less than the ultimate stress of the steel F_u, therefore justifying this common simplified representation of the stress-strain response.

2.2 Imperfections
Figures 1 (a), (b) and (c) show the initial out-of-flatness of the web, flange tilt and flange sweep assumed in this work. Only the flange sweep is used for rolled beams with compact webs while all three types of imperfection are used for members with non-compact webs. The flange sweep is sufficient to capture the dominant attributes of the response for compact-section beams; however, non-compact web members can be sensitive to the other imperfections as well.

(a): Web Out-of-flatness Imperfection

(b): Flange Tilt Imperfection   (c): Flange Sweep
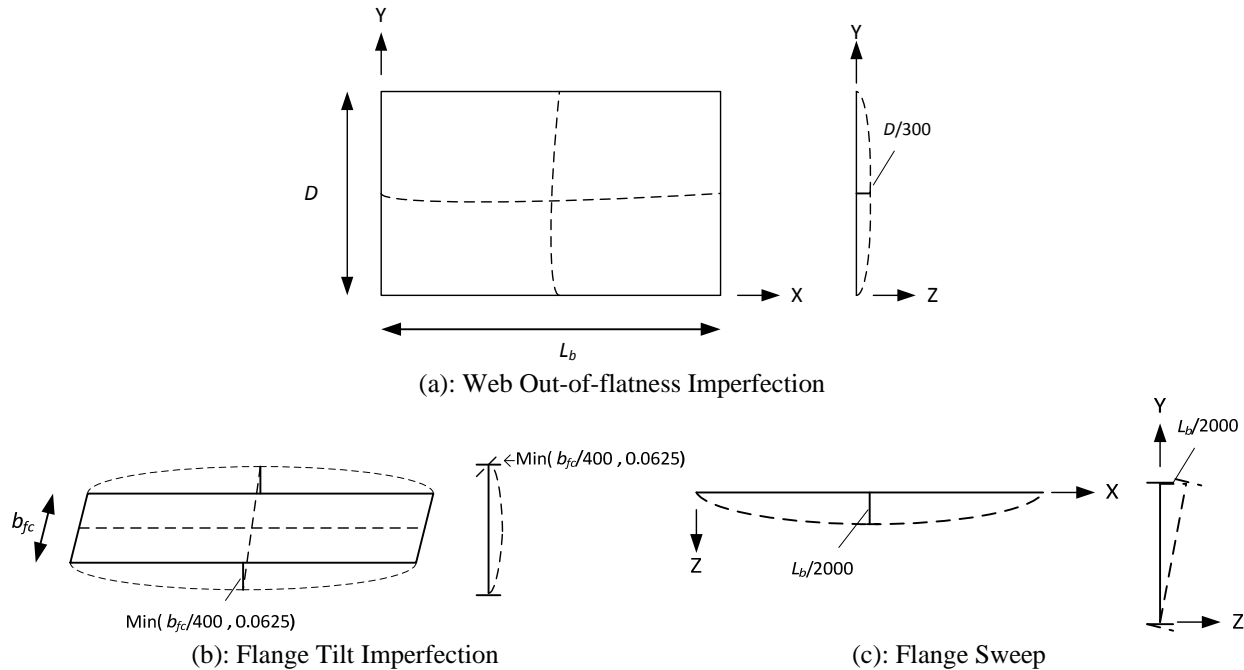
Figure 1: Initial Imperfections

AWS allows a maximum web out-of-flatness of $D/150$ for girders with no intermediate stiffeners and a flange tilt equal to the smaller of $b_{fc}/100$ and 0.25 in. The imperfection magnitudes shown in Figures 1(a) and 1(b) for the web out-of-flatness and flange tilt are half of those specified in AWS (2010) as the maximum allowed tolerance. In addition, AWS allows the maximum flange out-of straightness in beams or girders to be $L_b/960$, where L_b is the lateral unbraced length of the beam, whereas $L_b/2000$ is used for the simulations unless noted otherwise. It is shown that the assumption of the full tolerance values in simulations may be overly conservative. The three types of imperfections are superimposed in the same relative directions as shown in Figure 1. The sensitivity of the FEA test simulations to the flange sweep are presented below.
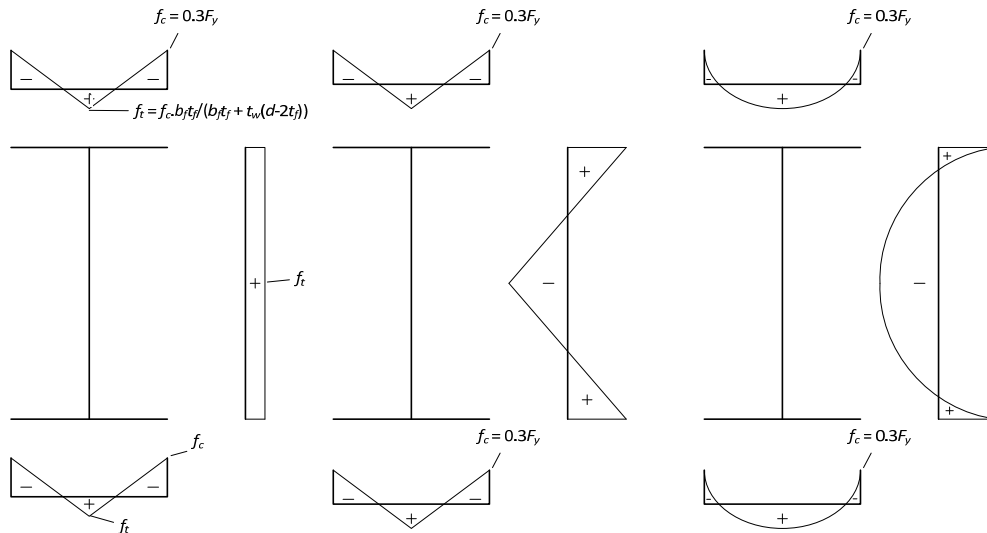
2.3 Residual Stress Patterns
Figure 2 shows various residual stress patterns used in the sensitivity studies presented in this paper. The Dux & Kitipornchai residual stresses shown in Figure 2(e) are measured values. It can be seen that these residual stresses are generally not in equilibrium. In using this residual stress pattern for the studies presented in this paper, the authors allowed the members to equilibrate under these stresses at zero applied loads in the FEA program. This means that the initial imperfections and residual stresses are slightly different from the nominal values assumed. The other residual stress patterns shown in Figure 2 are in equilibrium on the perfect member geometry.

2.4 Member Set-up
In the base studies conducted in this research, the test members are modeled as flexurally and torsionally simply-supported units with twist and lateral deflection restrained at the ends (fork boundary conditions). Two-sided transverse stiffeners are provided at the ends. Equal and opposite end moments are applied at the member ends and Vlassov kinematics are enforced at the member ends by the use of multi-point constraints. The effective length factor K for these members is one. In addition, simulation studies are conducted on selected experimental tests to

help identify FEA residual stresses and geometric imperfections that are not overly conservative, accounting for the higher capacities traditionally obtained in experimental tests when compared to test simulations.

(a): Lehigh(Galambos & Ketter, 1959) (b): ECCS (Boissonnade, et.al, 2002) (c): Polynomial (Szalai & Papp, 2004)
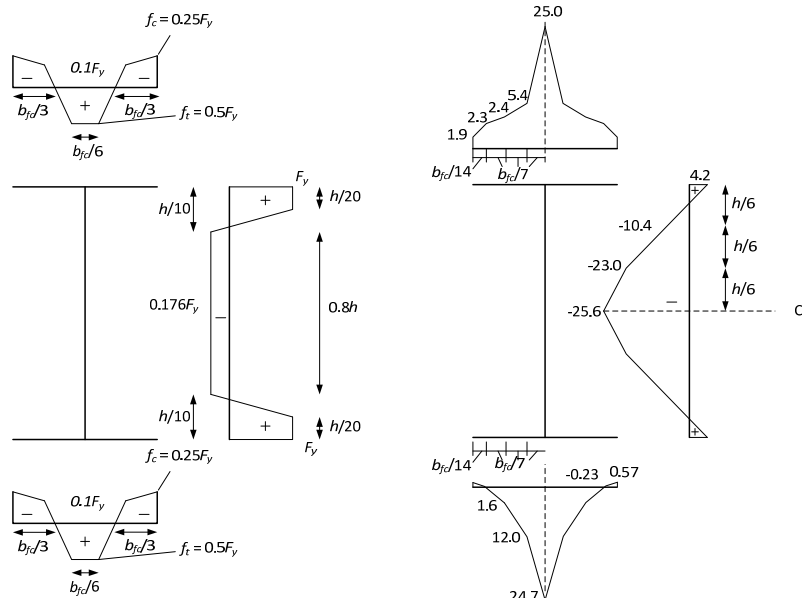
(d): Best Fit Prawel (Kim, 2010)   (e): Dux & Kit (Dux and Kitipornchai, 1983)

Figure 2: Residual Stress Patterns

3. Imperfection and Residual Stress Sensitivities on Rolled Beams and Plate Girders

In the following section, LTB curves are generated using FEA test simulations for two rolled sections and two plate girders with the various residual stress patterns shown in Figure 2 and the imperfections shown in Figure 1. Four different magnitudes of flange sweep are studied: $L_b/1000$, $L_b/2000$, $L_b/4000$ and $L_b/8000$. $L_b/8000$ may be considered as a negligible imperfection.

3.1 Sensitivity Studies on Rolled Beams

Sensitivity studies on two rolled beams, a W21x44 (D/b_{fc} = 3) and a W14x68 (D/b_{fc} = 1.3), are performed. The sensitivity of the rolled beam test simulation results to seven different nominal residual stress patterns is studied. The Lehigh residual stress in Figure 2(a) is considered with its full magnitude, half of its specified magnitude, and one quarter of its specified magnitude. In addition, the ECCS stress pattern in Figure 2(b), the polynomial stress pattern in Figure 2(c), a residual stress pattern measured by Dux and Kitipornchai (1983) shown in Figure 2(e), and a case with zero residual stresses are also considered.

Figures 3 and 4 show the results for a W21x44 with flange sweep of L_b/1000 and L_b/2000 for various residual stress patterns. Figures 5 and 6 show the results for a W21x44 for various imperfection magnitudes at half the Lehigh residual stress and at zero residual stress.
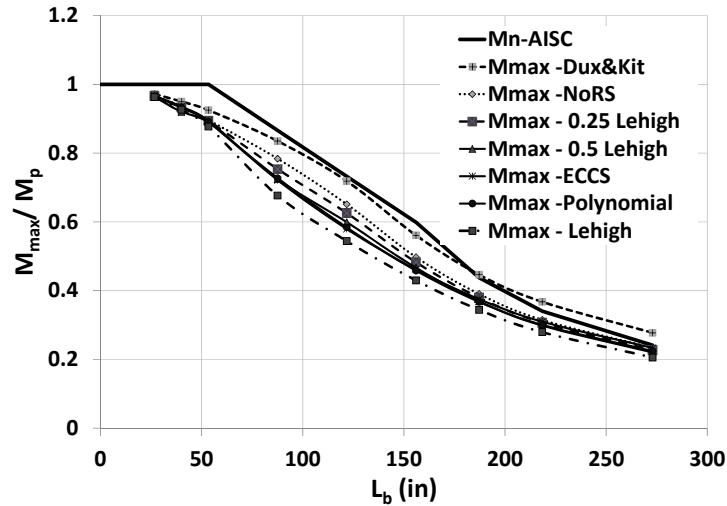

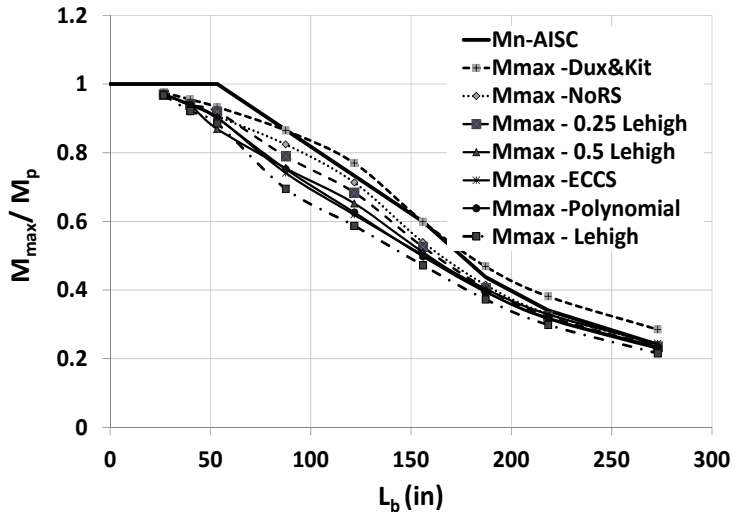Figure 3: LTB Curves for W21x44 with L_b/1000 Flange Sweep

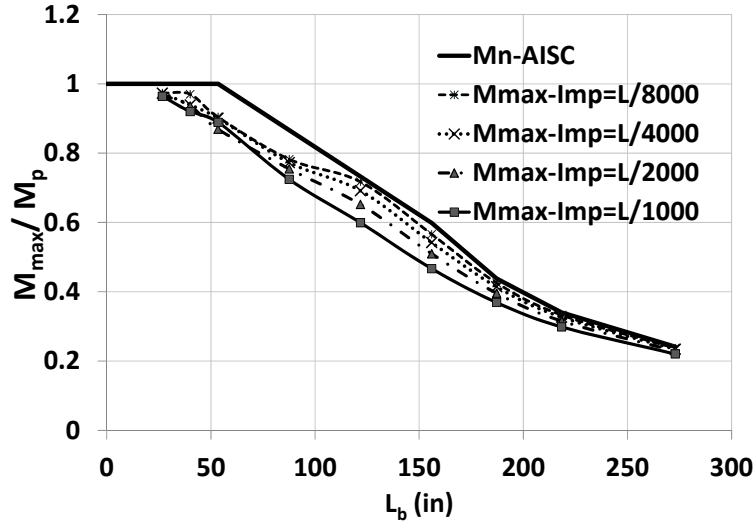Figure 4: LTB Curves for W21x44 with L_b/2000 Flange Sweep

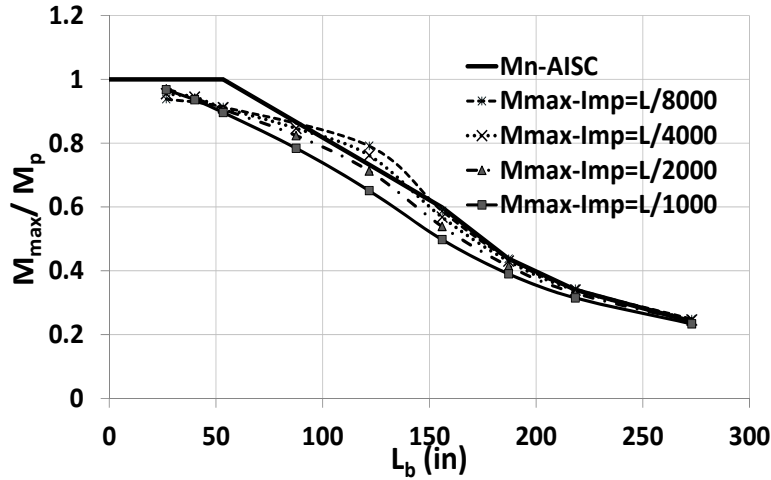Figure 5: LTB Curves for W21x44 with Half Lehigh Residual Stress

Figure 6: LTB Curves for W21x44 with Zero Residual Stress

It is observed that the sensitivity of the member capacities to the residual stress pattern and imperfection magnitude is most significant in the inelastic LTB region. The Lehigh residual stress pattern gives the lowest resistance for all imperfection magnitudes, while the residual stresses measured by Dux and Kitipornchai (1983) give the highest resistance. The relative effects of various residual stresses are essentially the same for imperfection magnitudes of $L_b/4000$ and $L_b/8000$. However, the capacities in these cases are closer to the AISC resistance curves. Plots for the W14x68 (not shown), which has a larger b_{fc}/D, show similar trends to the W21x44 curves. The "Dux & Kit" residual stresses often give resistances higher than the AISC resistance curve in the inelastic and elastic LTB ranges. This is due to the net tensile residual stresses in the flanges in these tests. Figures 5 and 6 show how the resistance increases with decreasing imperfection magnitude for a given residual stress pattern, and is especially sensitive in the inelastic LTB region. This behavior is typical of all the residual stresses studied in this paper. Clearly, it is imperative to choose an appropriate residual stress pattern and imperfection magnitude if test simulations are to be used to evaluate design LTB resistances.

It is observed that using the Lehigh pattern, which is a common residual stress pattern in North America for simulation studies on rolled beams, along with a flange sweep of $L_b/1000$, gives capacities up to 28% smaller than the AISC resistance equation in the inelastic region for the W21x44, and 19% less for the W14x68. Also, the AISC prediction with these parameters is 15% larger compared to the test simulation results in the elastic LTB region at a lateral unbraced length of $1.75L_r$ for the W21x44, while it is only 3% unconservative at an unbraced length of $1.75L_r$ for the W14x68. The plateau strength as per AISC for both these beams is less than 4% conservative at $0.5L_p$. However, as shown in Figures 3-6 and in Tables 1-4, the plastic moment is never reached in the FEA simulations at L_p, even in near-ideal cases with zero residual stress and imperfections of $L_b/8000$, i.e., a smaller unbraced length than L_p is needed to achieve M_p.

Tables 1-4 list the results obtained from FEA test simulations at four unbraced lengths for the two members as a function of the various residual stresses and imperfection magnitudes. The mean of the selected residual stress patterns is calculated neglecting the two case studies with flange tensile residual stresses and zero residual stresses. These two cases are neglected in order to focus on the effects of compressive flange residual stresses. The unbraced lengths L_p and L_r presented in the table represent the limiting unbraced lengths of the plateau region and the inelastic LTB region while $1.75L_r$ represents a point far into the elastic LTB region. In addition, the results are discussed for an intermediate unbraced length in the inelastic LTB region. Table 3 shows the results for an intermediate unbraced length in the inelastic LTB region, while Table 4 shows the results at L_r. Both tables show similar trends, with AISC tending to give larger resistances in the inelastic LTB region, as is also evident from Figures 3-6.

Table 1: $M_{max}/M_{n\,AISC}$ for W21x44 and W14x68 for different residual stresses and imperfection magnitudes at unbraced length L_p

Section	W21x44				W14 x68			
Imperfection	$L_b/1000$	$L_b/2000$	$L_b/4000$	$L_b/8000$	$L_b/1000$	$L_b/2000$	$L_b/4000$	$L_b/8000$
Lehigh	0.88	0.89	0.89	0.90	0.89	0.90	0.91	0.91
0.5 Lehigh	0.89	0.87	0.90	0.90	0.91	0.91	0.93	0.93
0.25 Lehigh	0.89	0.92	0.92	0.91	0.92	0.93	0.94	0.94
ECCS	0.89	0.90	0.91	0.91	0.91	0.92	0.93	0.93
Polynomial	0.89	0.90	0.90	0.91	0.92	0.93	0.94	0.95
Dux & Kit	0.93	0.93	0.94	0.94	0.94	0.95	0.96	0.96
Zero RS	0.90	0.91	0.91	0.91	0.93	0.94	0.95	0.95
Mean neglecting the Dux & Kit and Zero RS Cases	0.89	0.90	0.90	0.91	0.91	0.92	0.93	0.93

Table 2: $M_{max}/M_{n\,AISC}$ for W21x44 and W14x68 for different residual stresses and imperfection magnitudes at unbraced length $L_p + 2/3\,(L_r-L_p)$

Section	W21x44				W14 x68			
Imperfection	$L_b/1000$	$L_b/2000$	$L_b/4000$	$L_b/8000$	$L_b/1000$	$L_b/2000$	$L_b/4000$	$L_b/8000$
Lehigh	0.74	0.80	0.84	0.87	0.81	0.86	0.90	0.93
0.5 Lehigh	0.82	0.89	0.94	0.98	0.88	0.94	1.00	1.04
0.25 Lehigh	0.85	0.93	1.00	1.04	0.91	0.98	1.04	1.06
ECCS	0.79	0.85	0.88	0.90	0.84	0.89	0.93	0.95
Polynomial	0.80	0.85	0.89	0.92	0.87	0.92	0.96	0.98
Dux & Kit	0.98	1.05	1.10	1.14	0.97	1.05	1.11	1.12
Zero RS	0.89	0.97	1.04	1.08	0.94	1.02	1.06	1.12
Mean neglecting the Dux & Kit and Zero RS Cases	0.80	0.86	0.91	0.94	0.86	0.92	0.96	0.99

Table 3: $M_{max}/M_{n\,AISC}$ for W21x44 and W14x68 for different residual stresses and imperfection magnitudes at unbraced length L_r

Section	W21x44				W14 x68			
Imperfection	$L_b/1000$	$L_b/2000$	$L_b/4000$	$L_b/8000$	$L_b/1000$	$L_b/2000$	$L_b/4000$	$L_b/8000$
Lehigh	0.72	0.79	0.84	0.89	0.81	0.86	0.91	0.95
0.5 Lehigh	0.78	0.85	0.91	0.95	0.86	0.92	0.97	1.00
0.25 Lehigh	0.81	0.88	0.93	0.96	0.88	0.95	0.99	1.02
ECCS	0.77	0.84	0.89	0.93	0.83	0.89	0.93	0.97
Polynomial	0.77	0.83	0.88	0.93	0.85	0.91	0.95	0.99
Dux & Kit	0.94	1.00	1.05	1.07	0.95	1.01	1.05	1.07
Zero RS	0.83	0.90	0.95	0.98	0.91	0.97	1.01	1.03
Mean neglecting the Dux & Kit and Zero RS Cases	0.77	0.84	0.89	0.93	0.85	0.90	0.95	0.99

Table 4: $M_{max}/M_{n\,AISC}$ for W21x44 and W14x68 for different residual stresses and imperfection magnitudes at unbraced length $1.75L_r$

Section	W21x44				W14 x68			
Imperfection	$L_b/1000$	$L_b/2000$	$L_b/4000$	$L_b/8000$	$L_b/1000$	$L_b/2000$	$L_b/4000$	$L_b/8000$
Lehigh	0.85	0.89	0.92	0.94	0.97	1.04	1.05	1.06
0.5 Lehigh	0.91	0.95	0.97	0.98	1.00	1.09	1.10	1.10
0.25 Lehigh	0.94	0.97	0.99	1.00	1.09	1.11	1.12	1.12
ECCS	0.97	1.01	1.04	1.05	1.06	1.08	1.08	1.08
Polynomial	0.93	1.01	1.00	0.97	1.08	1.09	1.10	1.11
Dux & Kit	1.15	1.21	1.20	1.18	1.15	1.17	1.18	1.19
Zero RS	0.97	1.03	1.02	1.00	1.01	1.13	1.14	1.14
Mean neglecting the Dux & Kit and Zero RS Cases	0.92	0.97	0.98	0.99	1.04	1.08	1.09	1.09

The following observations can be made from Tables 1-4, and Figures 3-6.
1. The plateau strength, taken as the strength achieved for the smallest unbraced length considered, is insensitive to the imperfection magnitude or residual stress pattern.
2. The plastic moment capacity is never reached by either rolled beam at L_p, even for zero residual stress and near zero imperfections.
3. AISC is unconservative by an average of 10 % for the residual stresses and geometric imperfections considered, compared to FEA simulations for rolled beams at L_p. This suggests that the actual plateau strength for beams having an effective length factor, $K = 1$ is shorter than that specified by the design curves. Since the AISC curves are calibrated to experimental data, the specified plateau length would appear to be a result of incidental and unquantified additional restraints arising from adjacent segments and test apparatus. Although calibrating the AISC design curves to experimental data has its merits, it is worthwhile to assess the appropriate K factor to assume for incidental restraints, and whether that K should be built implicitly into the design equations or left to the judgment of the engineer.
4. The elastic LTB strengths specified by AISC for doubly-symmetric compact-web rolled beams is a very good prediction, except for the cases having $D/b_{fc}=3$, along with the Lehigh residual stress pattern.
5. The AISC curves tend to perform better on average for rolled beams with a larger b_{fc}/D (the W14x68) than for the beams with a smaller b_{fc}/D (the W21x44, $D/b_{fc}=3$).
6. The test simulation resistances are highly sensitive to geometric imperfections and residual stresses in the inelastic LTB region. The resistances from AISC curves are

especially high relative to the simulation results for the narrower flange rolled sections having compressive flange residual stresses.

7. The imperfection magnitude of $L_b/2000$ combined with one-half of the Lehigh residual stresses appears to provide the best correlation with the AISC/AASHTO LTB resistance curves. Combinations more severe than these result in conservative simulation studies that are inconsistent with available experimental data in a large number of cases. In addition, these are logical values for calculation of mean results from experimental tests, which often have imperfections and residual stresses that are less severe than the fabrication tolerances and the Lehigh residual stress pattern. Imperfection or residual stress magnitudes lower than these are too low, and do not seem appropriate to calibrate design curves.

3.2 Sensitivity Studies on Welded Plate Girders

Sensitivity studies on a non-compact web, compact flange welded plate girder (PG1) are performed. The girder PG1 is doubly symmetric with $D = 150$ inches, $D/t_w = 130$, $D/b_{fc} = 6$, and $b_{fc}/2t_{fc} = 9$. R_{pc} for this girder is 1.01. Hence, its theoretical plateau capacity is essentially M_y. The sensitivity of the test strengths to three different nominal residual stress patterns is studied: the Best-Fit Prawel residual stress in Figure 2(d) with its full magnitude, half of its magnitude, and with zero residual stresses. The four imperfection magnitudes of $L_b/1000$, $L_b/2000$, $L_b/4000$ and $L_b/8000$ on the flange sweep considered for the rolled beams are studied here as well. In addition, the imperfections include the flange tilt and web out-of-flatness with the magnitudes shown in Figure 1.

Figures 7 and 8 show the results for PG1 with a flange sweep of $L_b/1000$ and $L_b/2000$ for various residual stress patterns. Figures 9 and 10 show the results for PG1 with various imperfection magnitudes at half Best-Fit Prawel residual stress and zero residual stress.
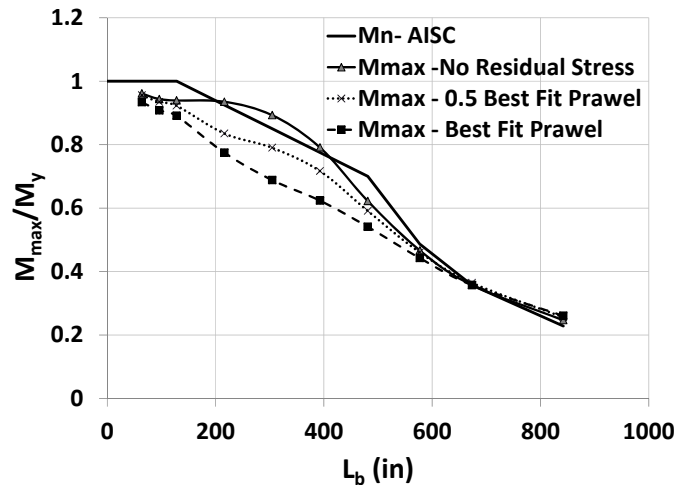

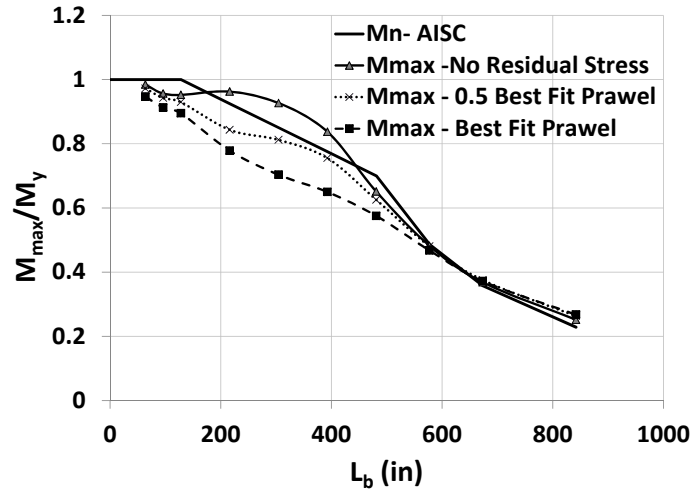Figure 7: LTB Curves for PG1 with $L_b/1000$ Flange Sweep

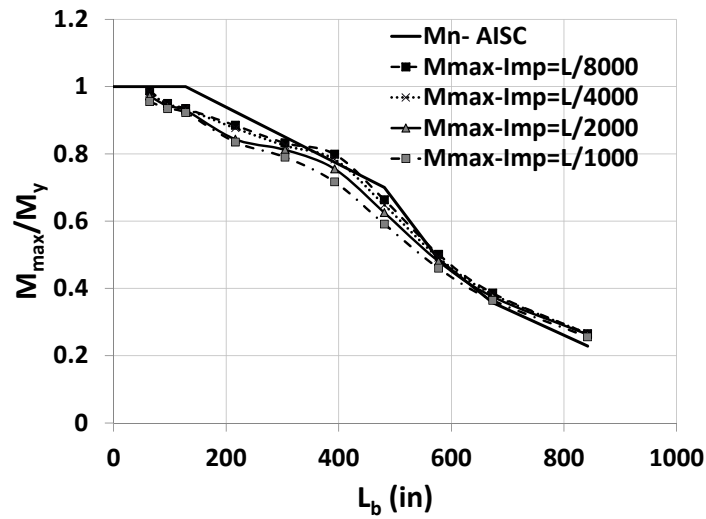Figure 8: LTB Curves for PG1 with L_b/2000 Flange Sweep

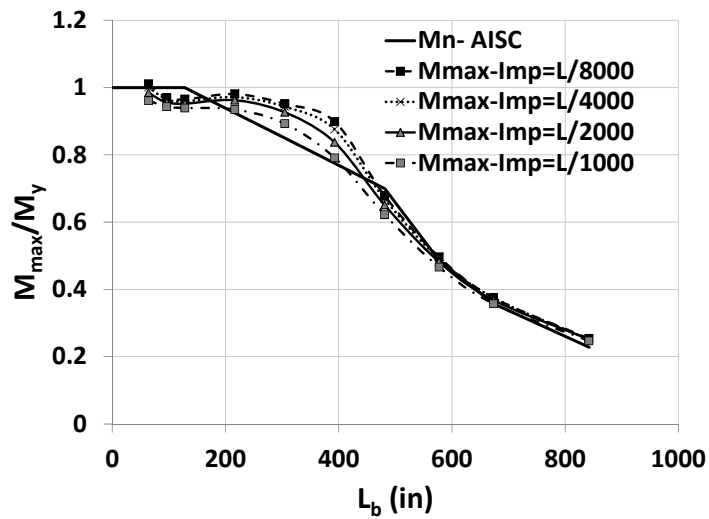Figure 9: LTB Curves for PG1 with Half Best-Fit Prawel Residual Stress

Figure 10: LTB Curves for PG1 with Zero Residual Stress

11

It is observed, as before, that the sensitivity of the capacities to the residual stress pattern or imperfection magnitude is significant in the inelastic LTB region. The Best-Fit Prawel residual stress pattern gives the lowest resistance for any imperfection magnitude. The relative effects of various residual stresses are the same for imperfection magnitudes of $L_b/4000$ and $L_b/8000$. However, the capacities in these cases are larger in the inelastic LTB region than for the cases with smaller imperfection magnitudes.

Tables 5-8 list the results obtained from FEA test simulations at four unbraced lengths for PG1 as a function of the different residual stress and imperfection magnitudes.

Table 5: $M_{max}/M_{n\,AISC}$ for PG1 for different residual stresses and imperfection magnitudes at unbraced length L_p

Imperfection	$L_b/1000$	$L_b/2000$	$L_b/4000$	$L_b/8000$
Best-Fit Prawel	0.89	0.89	0.90	0.90
0.5 Best-Fit Prawel	0.92	0.93	0.93	0.93
Zero RS	0.94	0.95	0.96	0.96
Mean neglecting the case with Zero RS	0.91	0.91	0.91	0.91

Table 6: $M_{max}/M_{n\,AISC}$ for PG1 for different residual stresses and imperfection magnitudes at unbraced length $L_p + 1/2\,(L_r-L_p)$

Imperfection	$L_b/1000$	$L_b/2000$	$L_b/4000$	$L_b/8000$
Best-Fit Prawel	0.81	0.83	0.84	0.84
0.5 Best-Fit Prawel	0.93	0.95	0.97	0.98
Zero RS	1.05	1.09	1.11	1.12
Mean neglecting the case with Zero RS	0.87	0.89	0.90	0.91

Table 7: $M_{max}/M_{n\,AISC}$ for PG1 for different residual stresses and imperfection magnitudes at unbraced length L_r

Imperfection	$L_b/1000$	$L_b/2000$	$L_b/4000$	$L_b/8000$
Best-Fit Prawel	0.77	0.82	0.85	0.87
0.5 Best-Fit Prawel	0.84	0.89	0.92	0.95
Zero RS	0.89	0.93	0.95	0.97
Mean neglecting the case with Zero RS	0.81	0.86	0.89	0.91

Table 8: $M_{max}/M_{n\,AISC}$ for PG1 for different residual stresses and imperfection magnitudes at unbraced length $1.5L_r$

Imperfection	$L_b/1000$	$L_b/2000$	$L_b/4000$	$L_b/8000$
Best-Fit Prawel	1.07	1.09	1.11	1.12
0.5 Best-Fit Prawel	1.05	1.08	1.08	1.08
Zero RS	1.01	1.03	1.03	1.04
Mean neglecting the case with Zero RS	1.07	1.09	1.11	1.12

The following observations can be made from Tables 5-8, and Figures 7-10.
1. As in the case of rolled beams, the plateau strength is insensitive to the imperfection magnitude or the residual stress pattern.
2. The plateau moment capacity is achieved by the non-compact plate girder at L_p only under ideal conditions of zero residual stress and near zero imperfection.
3. Similar to the observation on rolled beams, AISC is unconservative by an average of 10% at L_p. The capacity quickly drops off for $L_b > 0.5L_p$ for both compact rolled beams and non-compact web plate girders. This reinforces the hypothesis that the specified plateau length is a result of additional incidental restraints inherent in the experimental tests. These unquantifiable additional restraints cause a major disconnect between the use of

the experimentally based resistance curves and the use of test simulation to quantify resistances. It can be argued that it would be more appropriate to account for these effects by an explicitly stated $K < 1$ in the design calculations, where appropriate, rather than including these restraint effects implicitly within the strength curves.

4. The elastic LTB strengths specified by AISC are an accurate prediction for doubly-symmetric non-compact web plate girders.

5. Imperfection magnitude of $L_b/2000$ and half Best-Fit Prawel residual stresses appear to be reasonable FEA modeling parameters to use for LTB simulation studies on plate girders, to achieve reasonable consistency with available experimental data. In addition, these are logical values for calculation of mean results from experimental tests, which often have imperfections and residual stresses that are less severe than the fabrication tolerances and the Best-Fit Prawel residual stress pattern.

4. Imperfection and Residual Stress Sensitivities on Experimental Tests

A total of eight uniform bending experimental tests with compact and non-compact webs also have been modeled, using various imperfection magnitudes and residual stresses, to determine the conditions in which the simulation results predict the reported experiment values with greatest accuracy. This is done to verify that the simulation parameters of half-Lehigh/ half-Best-Fit Prawel residual stresses along with $L_b/2000$ as the initial flange sweep do not lead to overly unconservative predictions relative to the experimental results. The complete details of the test configurations and dimensions are catalogued in White and Jung (2004). Table 9 lists the tests modeled in the simulation studies, and the expected failure modes as per the AISC equations.

Table 9: Experimental tests modeled in FEA test simulations

Reference	Section Type	Test No	Flange	Web	Failure Mode	Designation in Paper
Adams, et al (1964)	Rolled	HT 29	Compact	Compact	Plastic Moment	HT 29
	Rolled	HT 36	Compact	Compact	Inelastic LTB	HT 36
Dux & Kitipornchai (1983)	Rolled	6	Compact	Compact	Inelastic LTB	DK 6
Wong-Chung & Kitipornchai (1987)	Rolled	1	Compact	Compact	Inelastic LTB	WK 1
	Rolled	5	Compact	Compact	Inelastic LTB	WK 5
	Rolled	9	Compact	Compact	Inelastic LTB	WK 9
Richter (1998)	Welded	5	Compact	Non-compact	Inelastic LTB	R5
	Welded	9	Compact	Non-compact	Inelastic LTB	R9

Tables 10-12 list the results for the sensitivity studies conducted on experimental tests that fail by inelastic LTB. Adam's tests HT 29 and HT36 have L_b very close to L_p and is discussed separately. It can be observed that using the half Best-Fit Prawel residual stresses or half Lehigh residual stresses along with a flange sweep of $L_b/2000$ gives the best correlation with the reported experimental tests of the parameters considered. Thus, these residual stresses along with $L_b/2000$ flange sweep would appear to be good choices for parametric studies to investigate other impacts on LTB resistances.

Table 10: M_{max}/M_{Exp} using Best-Fit Prawel and half Best-Fit Prawel residual stresses

Residual Stress	Best -fit Prawel				Half Best-Fit Prawel			
Imperfection	$L_b/1000$	$L_b/2000$	$L_b/4000$	$L_b/8000$	$L_b/1000$	$L_b/2000$	$L_b/4000$	$L_b/8000$
DK 6	0.97	0.99	0.99	1.02	1.01	1.03	1.04	1.05
WK 1	0.84	0.89	0.93	0.94	0.91	0.95	0.96	0.96
WK 5	0.85	0.88	0.90	0.91	0.92	0.97	0.99	1.04
WK 9	0.94	0.95	0.96	0.97	0.97	1.00	1.01	0.33
R5	0.92	0.93	0.93	0.93	0.96	0.97	0.97	0.98
R9	0.77	0.84	0.87	0.92	0.85	0.97	0.93	1.01
Mean	0.88	0.91	0.93	0.95	0.94	0.98	0.98	0.89

Table 11: M_{max}/M_{Exp} using Lehigh and half Lehigh residual stresses

Residual Stress	Lehigh				Half Lehigh			
Imperfection	$L_b/1000$	$L_b/2000$	$L_b/4000$	$L_b/8000$	$L_b/1000$	$L_b/2000$	$L_b/4000$	$L_b/8000$
DK 6	0.95	0.97	0.98	0.99	0.99	1.02	1.03	1.05
WK 1	0.84	0.89	0.92	0.93	0.90	0.95	0.96	0.96
WK 5	0.85	0.89	0.91	0.92	0.92	0.96	0.98	1.01
WK 9	0.92	0.94	0.95	0.96	0.97	0.99	0.98	1.01
R5	0.93	0.94	0.95	0.96	0.96	0.97	0.97	0.98
R9	0.77	0.79	0.84	0.89	0.83	0.92	0.97	1.00
Mean	0.88	0.90	0.93	0.94	0.93	0.97	0.98	1.00

Table 12: M_{max}/M_{Exp} using ECCS residual stresses

Residual Stress	ECCS			
Imperfection	$L_b/1000$	$L_b/2000$	$L_b/4000$	$L_b/8000$
DK 6	0.99	1.01	1.02	1.03
WK 1	0.87	0.91	0.93	0.96
WK 5	0.89	0.93	0.95	0.96
WK 9	0.96	0.98	0.99	1.00
R5	0.95	0.96	0.96	0.97
R9	0.81	0.87	0.90	0.92
Mean	0.91	0.94	0.96	0.97

Tests HT29 and HT36 have $L_b \cong L_p$, where L_p is defined as $1.1r_t\sqrt{E/F_y}$. The test configuration is a 4-point bending with the loads at the one-third points. This gives uniform moment in the middle unbraced length while the adjacent segments are less severely loaded and are subjected to moment gradient. The theoretical elastic LTB K factor for this case is 0.83. It is observed that modeling the girder exactly using the configuration reported by Adams et al. gives the plastic moment capacity as reported by them. However, modeling an isolated beam with the same cross section, fork boundary conditions and an unbraced length of $0.83L_p$ similar to the base studies reported in this paper achieves only $0.95M_p$. It must be noted that the AISC equation of $L_p = 1.76r_y\sqrt{E/F_y}$ further increases the design plateau length for this girder by 1.4 times the previous equation. This suggests that the AISC equations inherently assume a K factor less than 1 via the calibration of L_p to experimental data, as discussed by White (2008).

5. Proposed Model

The above sections show that the AISC equations tend to give larger member capacities compared to simulation results at L_p and in the inelastic LTB region for both compact and non-compact webs. It is also noted that the estimates from the Specification equations are more accurate for sections with larger b_{fc}/D. The magnitude of the disconnect between test simulation results and the Specification strength curve in the inelastic LTB region is particularly worrisome. An approach to modify this curve is presented here as the Modified Kim method based on Kim (2010). In this proposed approach, a reduced value of L_p, $L_p = 0.63r_t\sqrt{E/F_y}$ (Kim, 2010), and a smaller maximum stress level for elastic LTB of $F_{yr} = 0.5F_y$ is recommended by the authors. The calculations from this model are presented for various compact-web rolled beams and non-compact web doubly-symmetric plate girders along with the FEA simulation data. In addition, comparisons are made to the current AISC and Eurocode (CEN 2006a & 2006b) provisions. For rolled sections, the larger of two available Eurocode predictions is shown. Table 13 lists the cross-sections for which the comparative studies are presented in this paper. The results are shown in Figures 11–19. The FEA simulation results for rolled beams are presented using half of the Lehigh residual stresses, while half of the Best-Fit Prawel residual stresses are used for plate girders. The imperfection magnitudes shown in Figure 1 are used in all the simulations.

Table 13: Members presented for comparative studies

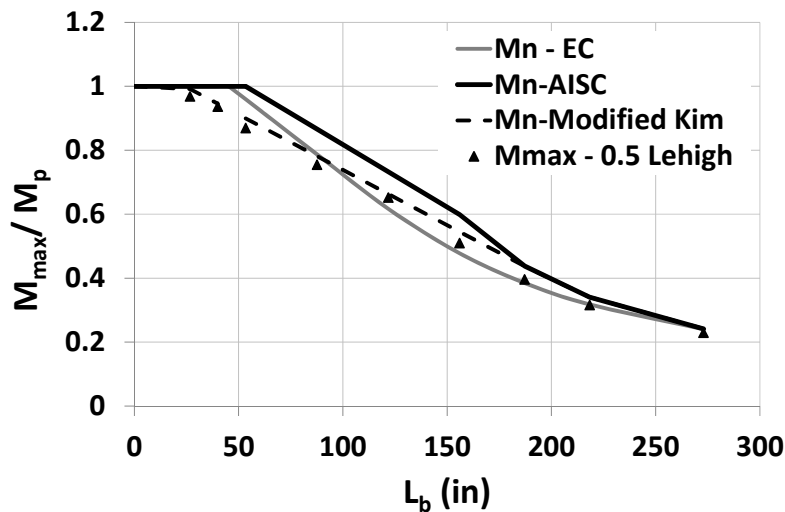| Section Type	Member	D/t_w	D/b_{fc}	$b_{fc}/2t_{fc}$	Web	Flange
Rolled Beams	W 21 x 44	57	3	7	Compact	Compact
	W 14 x 68	30	1.3	7	Compact	Compact
	W 10 x 30	32	1.6	6	Compact	Compact
	W 16 x 31	55	2.7	6	Compact	Compact
	W 14 x 90	29	0.9	10	Compact	Non-compact
Plate Girders	PG1	130	6	9	Non-compact	Compact
	PG2	130	5.4	11	Non-compact	Non-compact
	PG3	130	3	9	Non-compact	Compact
	PG4	130	3	11	Non-compact	Non-compact

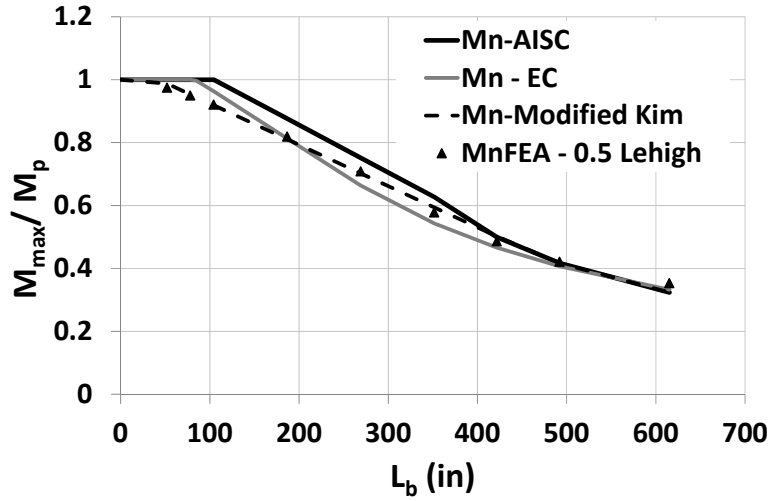Figure 11: LTB Curves for W21x44

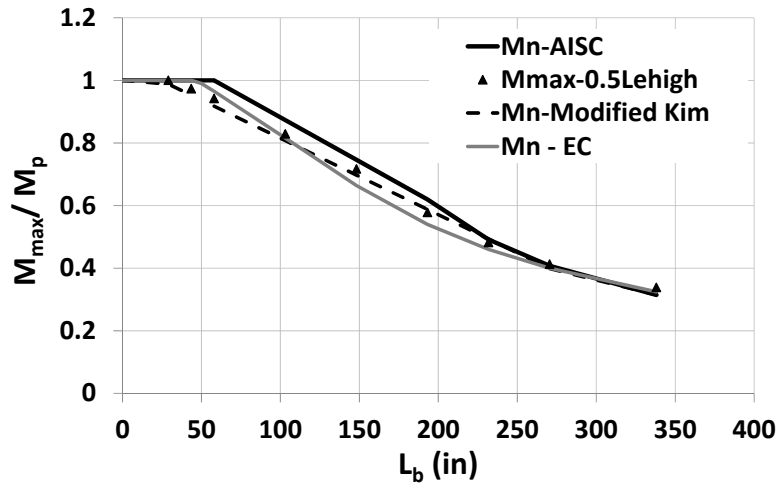Figure 12: LTB Curves for W14x68

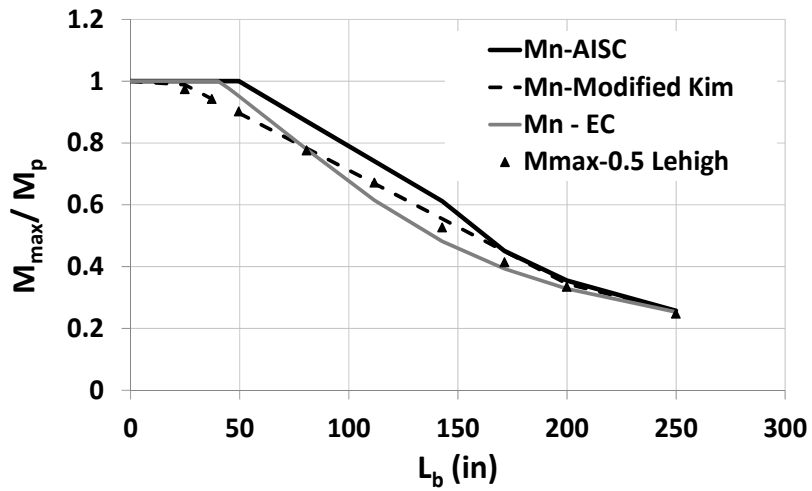
Figure 13: LTB Curves for W10x30
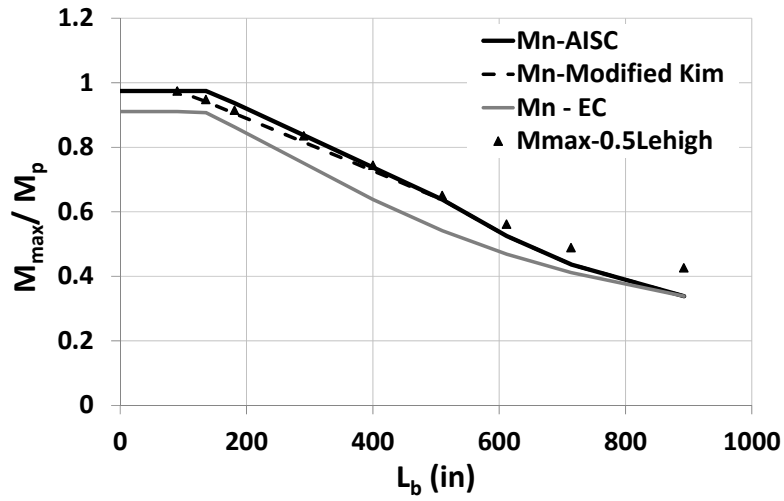

Figure 14: LTB Curves for W16x31
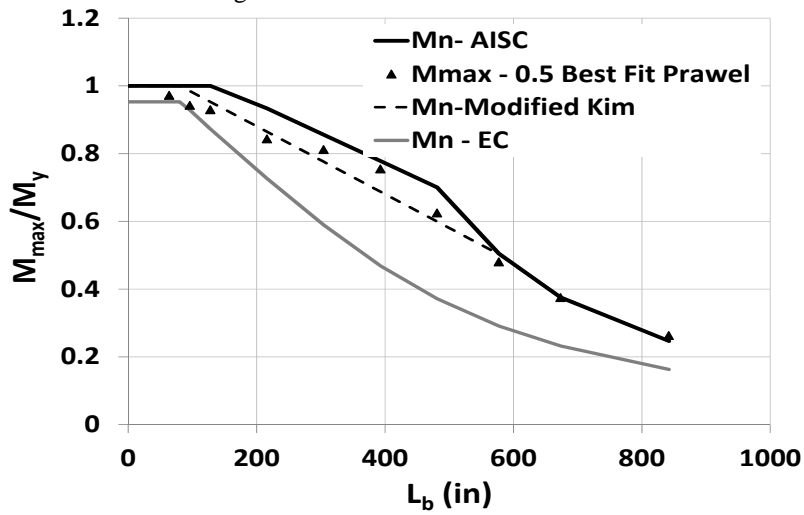
Figure 15: LTB Curves for W14x90
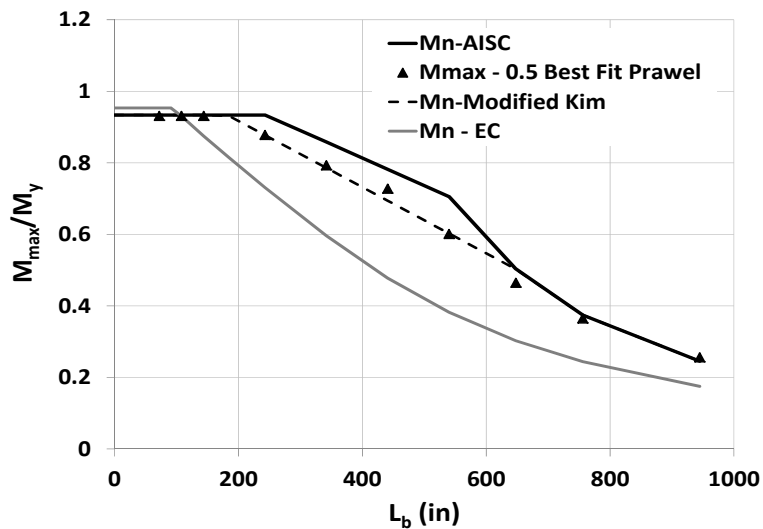

Figure 16: LTB Curves for PG1
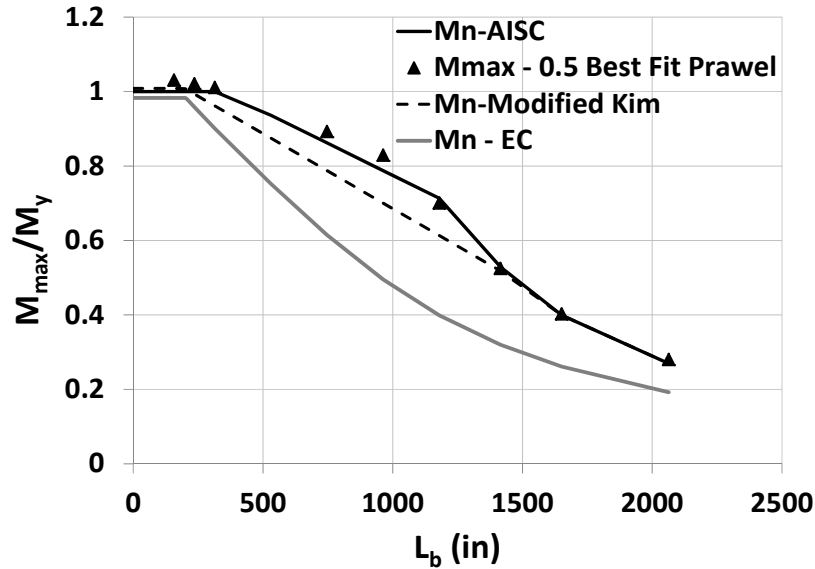

Figure 17: LTB Curves for PG2
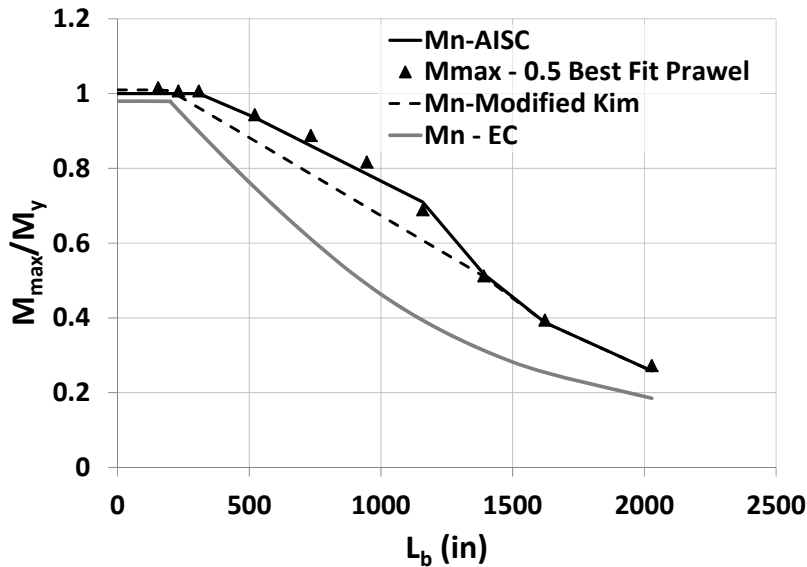
Figure 18: LTB Curves for PG3

Figure 19: LTB Curves for PG4

It can be seen from Figures 11-17 that the Modified Kim method gives very good correlation with FEA simulation data for all rolled beams and non-compact web plate girders with narrow flanges. It gives conservative estimates for plate girders PG3 and PG4, which have wider flanges, but also, the theoretical capacities for these girders are essentially M_y, as opposed to M_p for the rolled sections. For the plate girders with wider flanges ($D/b_{fc} = 3$), the data from the FEA simulations match well with the AISC curve. This indicates the possible need for further consideration of the influence of D/b_{fc} on the elastic and inelastic buckling strengths. However, the Modified Kim model is conservative by only a maximum of 13% in both PG3 and PG4 in the inelastic buckling region. It may be argued that this is an improvement over the AISC equations, which give significantly larger strengths (~ 30% larger) relative to test simulations as discussed in Section 3. The AISC equations give larger strengths throughout the inelastic LTB region compared to the test simulations.

6. Conclusions

1. The frequent observation of a disconnect between FEA test simulation results and current AISC/AASHTO curves has been addressed by means of comprehensive sensitivity studies on imperfections and residual stresses. The use of half Lehigh residual stresses for rolled beams and half of Best-Fit Prawel residual stresses for welded girders along with half of the recommended AWS tolerances for imperfections is recommended as FEA modeling parameters to calibrate to the AISC/AASHTO curves that have been established based on experimental data. The appropriate selection of these parameters for simulation studies is extremely significant because of the high sensitivity of the strengths to these parameters within the inelastic buckling range. These residual stresses and geometric imperfections are more representative of the mean experimental test conditions captured by the AISC/AASHTO strength curves. The satisfactory correlation with key experimental data as shown in this paper gives further confidence in this approach of using reduced nominal residual stresses and geometric imperfections.

2. The simulation studies indicate an implicit K factor less than 1.0 in the AISC/AASHTO resistance equations. This produces consistently larger code strength values relative to test simulations at the limiting plateau length of L_p. This is resolved in the proposed resistance equations by reducing the parameter L_p. This is also justified from a comprehensive set of studies performed by Kim (2010).

3. The larger strength calculations by the code equations in the inelastic LTB region is addressed by reducing the maximum stress level for elastic LTB to $F_{yr} = 0.5F_y$. This results in slightly conservative estimates for sections with larger b_{fc}/D.

7. Future Work

The authors have conducted additional studies on singly-symmetric girders as well as slender web sections and longitudinally stiffened sections, including cases of non-uniform bending. The proposed model has been found to predict test results reasonably well. The proposed model can be improved by explicitly accounting for the influence of b_{fc}/D. These results will be discussed in subsequent papers by the authors.

References

AASHTO (2014). AASHTO LRFD Bridge Design Specifications. 7th Edition, American Association of State Highway and Transportation Officials, Washington, DC. U.S. customary and metric editions.

Adams, P. F., Lay, M. G., and Galambos, T. V.1964. "Experiments on high strength steel members," Fritz Engineering Laboratory Rep. No. 297.8, Lehigh Univ., Bethlehem, Pa.

AISC (2010). Specification for Structural Steel Buildings, ANSI/AISC 360-10, American Institute of Steel Construction, Chicago, IL.

AWS (2010). Structural Welding Code–Steel, AWS D1.1: D1.1M, 22nd ed., prepared by AWS Committee on Structural Welding, 572 pp.

Boissonnade,N., Jaspart, J.-P., Muzeau, J.-P., and Villette, M. (2002), "Improvement of the interaction formulae for beam columns in Eurocode 3," Computers & Structures, Volume 80, Issues 27–30, November, Pages 2375-2385.

CEN (2006a). Eurocode 3: Design of Steel Structures, Part 1-5: General Rules - Plated Structural Elements, EN 1993-1-5:2006: E, Incorporating Corrigendum April 2009, European Committee for Standardization, Brussels, Belgium, 56 pp.

CEN (2005). Eurocode 3: Design of Steel Structures, Part 1-1: General Rules and rules for buildings, EN 1993-1-1:2005:E, Incorporating Corrigendum February 2006, European Committee for Standardization, Brussels, Belgium, 91 pp.

Dux, P.F., and Kitipornchai, S. (1983), "Inelastic Beam Buckling Experiments," Journal of Constructional Steel Research, Vol. 3, No. 1, 3-9.

Galambos, T.V. and Ketter, R.L. (1959), "Columns Under Combined Bending and Thrust," Journal of the Engineering Mechanics Division, ASCE, 85(EM2), 135-152.

Greiner, R. and Kaim, P. (2001). "Comparison of LT-Buckling Design Curves with Test Results," ECCS TC8, Report 23, April, 23 pp.

Kim, Y.D. (2010). "Behavior and Design of Metal Building Frames Using General Prismatic and Web-Tapered Steel I-Section Members," Doctoral Dissertation, School of Civil and Environmental Engineering, Georgia Institute of Technology, Atlanta, GA.

Richter, J.F. (1998), "Flexural Capacity of Slender Web Plate Girders," M.S. Thesis, The University of Texas at Austin, Austin, TX, 133 pp.

Righman, J. (2005). "Rotation Compatibility Approach to Moment Redistribution for Design and Rating of Steel I-Girders, Doctoral Dissertation, Civil Engineerig, West Virginia University.

Simulia (2013). ABAQUS/Standard Version 6.12-1, Simulia, Inc. Providence, RI.

Szalai. J., and Papp.F. (2005), "A new residual stress distribution for hot-rolled I-shaped sections," Journal of Constructional Steel Research, Volume 61, Issue 6, June, Pages 845-861

White, D.W. (2008). "Unified Flexural Resistance Equations for Stability Design of Steel I-Section Members – Overview," Journal of Structural Engineering, ASCE, 134(9), 1405-1424.

White, D.W. and Jung, S.-K. (2004). "Unified Flexural Resistance Equations for Stability Design of Steel I-Section Members – Uniform Bending Tests," Structural Engineering, Mechanics and Materials Report No. 28, School of Civil and Environmental Engineering, Georgia Institute of Technology, Atlanta, GA.

Wong-Chung, A.D. and Kitipornchai, S. (1987), "Partially Braced Inelastic Beam Buckling Experiments," Journal of Constructional Steel Research, 7, 189-211.